

Effect of Al₂O₃ Micro-powder Additives on the Properties of Micro-arc Oxidation Coatings Formed on 6061 Aluminum Alloy

Ping Wang, Ting Wu, You Tao Xiao, Jun Pu, Xiao Yang Guo, Jun Huang, and Chun Lang Xiang

(Submitted April 5, 2016; in revised form July 11, 2016; published online July 29, 2016)

Al₂O₃ micro-powder was suspended in the basis electrolyte to form micro-arc oxidation (MAO) coatings on 6061 aluminum alloy by MAO. During the stage of micro-arc oxidation, Al₂O₃ micro-powder with negative surface charge was melted by the micro-arc around the anode and incorporated into the MAO coatings. With the continuous addition of Al₂O₃ micro-powder, the oxidation voltages rose up firstly and then decreased. The surface and cross-sectional morphologies showed that the size of micropores decreased and the MAO coatings surface got loosened following the variation in Al₂O₃ micro-powder concentration. As a consequence of the changing coating structure, the corrosion resistance of the coatings decreased apparently. The micro-hardness of the coatings increased firstly and then decreased, opposite to the trend of the average friction coefficient. It revealed the minimum average friction coefficient of MAO coatings and maximum adhesion between the coatings and substrate when 2.0 g/L Al₂O₃ micro-powder was added into electrolyte. There were visible cracks and peelings on the coating surface merely at 4.0 g/L after thermal shock tests. The x-ray diffraction results indicated that the addition of Al₂O₃ micro-powder had less effect on the phase composition of MAO coatings.

Keywords Al₂O₃ micro-powder, aluminum alloy, micro-arc oxidation, microstructure

1. Introduction

The widespread application of aluminum alloy has been restricted by its poor surface performance such as lower hardness and wear resistance, which exhibit extensive significance in practical application (Ref 1, 2). Thus, it is imperative to enhance its surface properties to meet the ever-increasing demands. Focused on the latest surface treatment technology, micro-arc oxidation (MAO) is a desirable method to coat aluminum materials via environmental-friendly process and attain required corrosion and wear resistance by one step (Ref 3, 4). The main composition of MAO coatings on aluminum alloy is Al₂O₃, which can markedly improve their surface mechanical properties (Ref 5-8). Meanwhile, Al₂O₃ particles always serve as wear-proof and corrosion-proof materials in industry. Therefore, an on-going thought was put forward that we could try to add Al₂O₃ particles into the basis electrolytes for further improving the properties of aluminum alloy by MAO process.

Contemporarily, the investigation of MAO focuses on adding different particles including SiC, ZrO₂, Al₂O₃, MgO and graphite into basis electrolytes to adjust the performance of MAO coatings (Ref 9-13). Xijin Li (Ref 10) found that Al₂O₃ particles doping in MAO coatings on AM60B magnesium alloy

increased the ratio of MgAl₂O₄/MgO and proposed a new chemical reaction mechanism for the incorporation of Al₂O₃ in the MAO coatings. So far, the uptake and incorporation of Al₂O₃ particles during MAO process on aluminum alloy have been rarely reported. In this study, the micro-arc oxidation (MAO) coatings were fabricated on 6061 aluminum alloy in the electrolytes containing Al₂O₃ micro-powder 0, 2.0, 4.0, 6.0, 8.0 g/L. The effects of Al₂O₃ concentration in electrolytes on the characteristics of MAO coatings were investigated, and the doping mechanism of Al₂O₃ micro-powder was also discussed.

2. Experimental

Rectangular specimens (10 mm × 10 mm × 3 mm) of 6061 aluminum alloy were used as the substrates for MAO experiments. The nominal composition (mass fraction) of 6061 aluminum alloy is Mg 0.8-1.2%, Si 0.40-0.80%, Cu 0.15-1.40%, Fe 0.00-0.70%, Cr 0.04-0.35%, Zn ≤ 0.25%, Mn ≤ 0.15%, Ti ≤ 0.15% and Al balance. The basis electrolyte was consisted of 10 g/L Na₂SiO₃, 0.1 g/L NaOH, 3 ml/L C₃H₈O₃. The Al₂O₃ micro-powder (grain diameter 20-100 μm) was stirred continuously during the treatment in order to keep homogeneous in the electrolytes varied from 0 to 8.0 g/L. The MAO process was carried out using a pulsed electrical power to provide positive pulse voltage. The MAO coatings were obtained under peak anodic current density of 3A/dm² for 20 min, with fixed frequency of 100 Hz and duty cycle of 40%. The electrolytes temperature was kept below 30 °C by a heat exchange system during the MAO process. After MAO treatment, samples were rinsed with hot water at 90 °C and dried in warm air.

A Scanning Electron Microscope (SEM, FEI Quanta 450) was employed to study the surface and cross-sectional

Ping Wang, Ting Wu, You Tao Xiao, Jun Pu, Xiao Yang Guo, Jun Huang, and Chun Lang Xiang, College of Materials Science and Engineering, Southwest Petroleum University, Chengdu 610500, China. Contact e-mail: 818wp@163.com.

morphologies of MAO coatings. The distribution of aluminum and oxygen was determined by energy dispersive spectrometer (EDS, EMAXGENESIS). The phase composition of the coatings was investigated by x-ray diffraction (XRD, DX-1000). Diffraction data were acquired over scattering angle 2θ from 10° to 80° , scanning speed was $0.1^\circ/\text{s}$. ZETA Potential Meter (ZetaProbe) was applied to analyze the surface charge of Al_2O_3 micro-powder in the electrolytes. The polarization curves, surface micro-hardness and thickness of MAO coatings were investigated by Electrochemical Workstation (IM6), digital micro-hardness tester (HVS-1000) at 1 N for 15 s and digital thickness gauges (TT230) severally. Furthermore, the scratch tests of the coatings which could evaluate the adhesion between substrate and coatings were carried out by multifunctional surface performance tester (MFT-4000) with the automatic loading from 0 to 100 N; loading rate was 0.5 N/s. The average friction coefficient of the coatings was detected at 2 N by friction and wear spectrometer (MS-T3000), and the thermal shock tests of the coatings were studied by chamber electric furnace (SX-10-12) at 500°C for 5 min and then cooled down in 25°C water for 50 cycles.

3. Results and Discussion

Figure 1 shows that the oxidation voltage improved at first and then declined gradually with the increase of Al_2O_3 micro-powder. The surface charge of Al_2O_3 micro-powder in electrolytes measured by ZETA Potential Meter was -0.5 mV and Al_2O_3 micro-powder moved toward the anode with the effect of electric field and mechanical stirring. When 2.0 g/L Al_2O_3 micro-powder was added into the electrolyte, the adsorption capacity of Al_2O_3 micro-powder on the specimen surface strengthened the electrical resistance giving rise to the rapid growth of oxidation voltage. Nevertheless, the continuous addition of Al_2O_3 micro-powder preferred to slow down the growth rate of oxidation voltage and the ultima oxidation voltage decreased gradually. The reason is that the abundant adsorption capacity of negative charged Al_2O_3 micro-powder on the anode specimens produced double electric fields with reverse directions between the specimens and the anode-electrolyte interface, resulting in the decrease in the electric potential on the specimens.

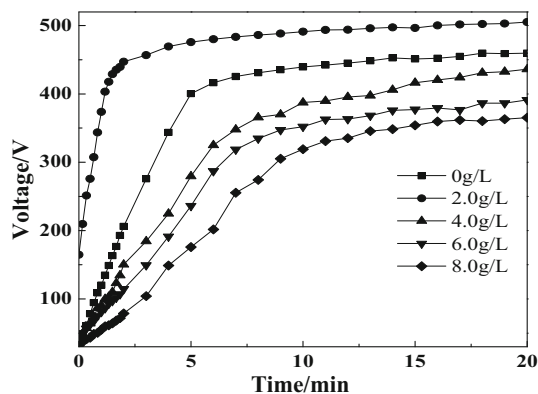
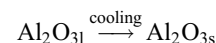
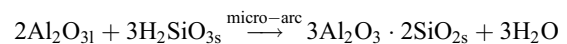
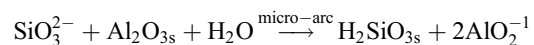
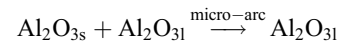
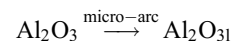
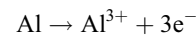


Fig. 1 Voltage–time plots at different Al_2O_3 micro-powder concentrations

Figure 2(a)–(j) presents the surface and cross-sectional microstructure of specimens at different Al_2O_3 micro-powder concentrations. A porous morphology of the coatings was observed without Al_2O_3 micro-powder added, revealing the interaction between high-heat electric arcs and cold electrolytes (Fig. 2a). From the SEM images, it was obvious that the size of micropores on MAO coatings shrunk gradually with the addition of Al_2O_3 micro-powder in comparison with that without Al_2O_3 micro-powder. The surface morphology converted porosity into laminate, even some loosened attachments appeared on the surface of the specimen at 8.0 g/L. Surface micro-hardness of the five specimens just ascended up at 2.0 g/L and decreased afterward (Fig. 3). The temperature of micro-areas caused by electric arcs surged to 10^3 – 10^4 K (Ref 1) during the spark discharge process, which was adequate to melt both micro-areas of the coatings and the adsorbed Al_2O_3 micro-powder. At first, the melted Al_2O_3 micro-powder filled up the discharge channels, which decreased the micropore size and improved the surface homogeneity and hardness of the coatings. Then, the more Al_2O_3 additives are added, and the more heat is absorbed. The effect of the fusion energy on the added Al_2O_3 micro-powder weakened and the combination mode between Al_2O_3 micro-powder and Al_2O_3 coating formed by aluminum substrate oxidized was no longer atom bonding, because the oxidation voltage decreased constantly. The loosened attachments which were proved to be mullite ($3\text{Al}_2\text{O}_3 \cdot 2\text{SiO}_2$) analyzed by EDS, generated on MAO coating surface (Fig. 2i) with the decrease in surface micro-hardness. As a consequence, the average friction coefficient revealed increase after 2.0 g/L (Fig. 3).

The Al_2O_3 micro-powder with negative surface charge was easily incorporated in the surface of oxidation coatings by the interaction of electric field and mechanical stirring. During the micro-arc oxidation stage, the Al_2O_3 micro-powder and MAO coatings were melted together via local high temperature produced by micro-arcs and then cooled down by the electrolytes. Passing through the stage, the combination between a part of Al_2O_3 micro-powder and oxidative substrate came into atom bonding. The possible reactions are as follows:



The thickness of MAO coatings tended to rise up firstly and then decline from 6.0 g/L (Fig. 2b, d, f, h, j). The uniformity of the coatings decreased accompanying with some strip cracks generated in the coatings gradually (Fig. 2f). Some Al_2O_3 micro-powder and coatings sintered to blocks. The reason was that the Al_2O_3 micro-powder was too much to be melted completely in time and not reacted sufficiently, which resulted that the coating surface was thick but loose. The moderate

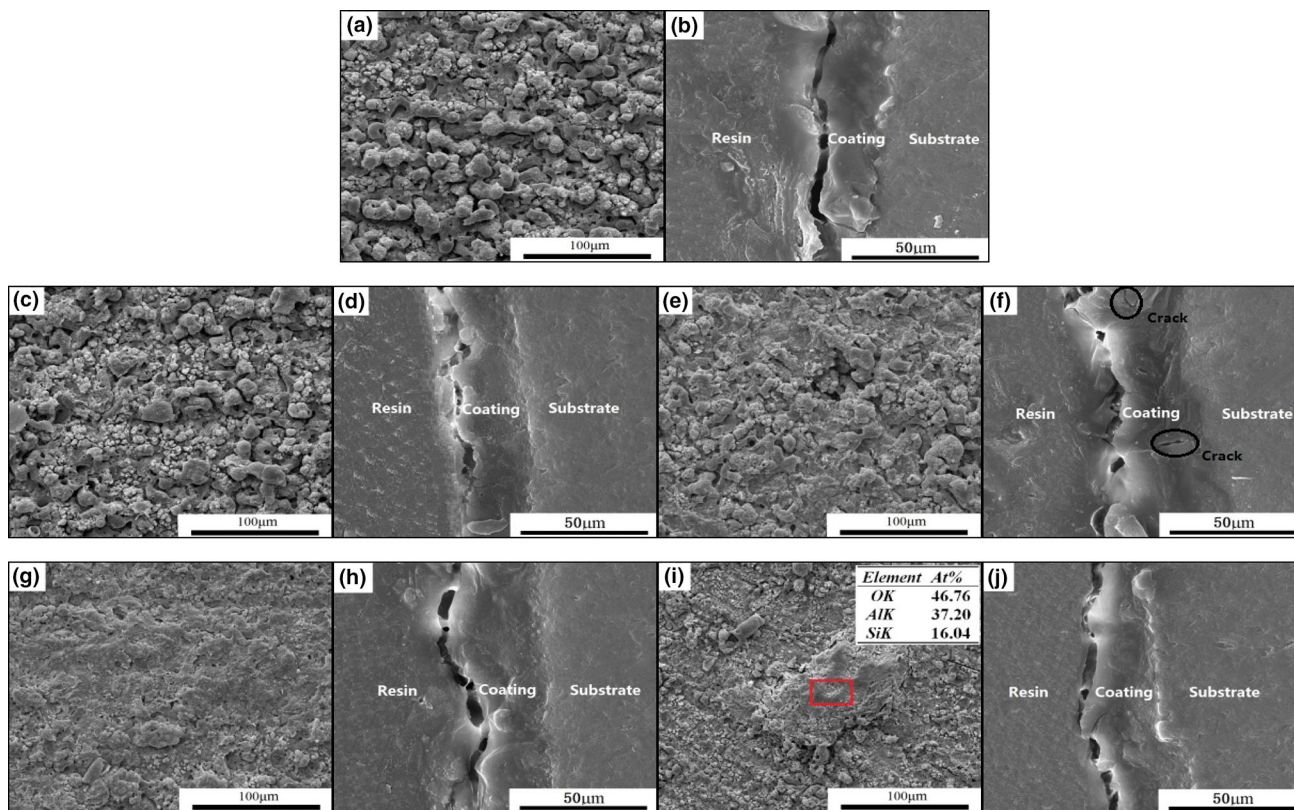


Fig. 2 Surface and cross-sectional morphologies of MAO coatings at different Al_2O_3 concentrations: (a, b) 0 g/L; (c, d) 2.0 g/L; (e, f) 4.0 g/L; (g, h) 6.0 g/L; (i, j) 8.0 g/L

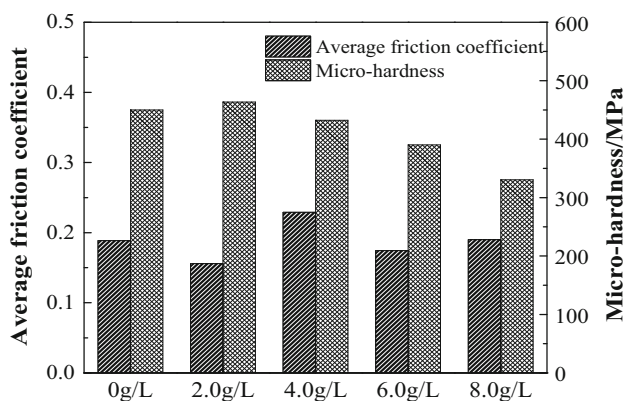


Fig. 3 Variation in the average friction coefficient and micro-hardness of MAO coatings at different Al_2O_3 micro-powder concentrations

Al_2O_3 micro-powder additives facilitated the formation of MAO coatings, which demonstrated that Al_2O_3 micro-powder involved in the formation of new coatings in collaboration with the Al_2O_3 coatings produced by oxidative substrate. The process improved utilization of the heat and reduced MAO energy consumption effectively. Although there were some cracks caused by the thermal shrinkage of the resin between MAO coatings and resin, the combination between the coatings and the substrate was tight without any cracks yet.

From Fig. 4, it is evident that the critical load of the coatings increased with the addition of Al_2O_3 micro-powder in electrolytes,

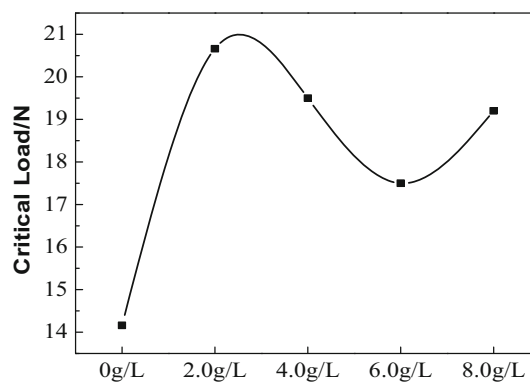


Fig. 4 Variation in the critical load when the coatings were destroyed exactly at different Al_2O_3 concentrations

when the MAO coatings were destroyed exactly during the scratch tests. Generally, the value of critical load is used to evaluate the adhesion between substrates and coatings and changed in direct proportion to the adhesion. Therefore, the adhesive strength between the substrates and coatings was enhanced after the addition of Al_2O_3 micro-powder. The improvement in the adhesion could be attributed to the variation in the residual stress and the thickness of the coatings. When Al_2O_3 micro-powder added, the electric energy distributed more uniformly on the coatings and then the residual stress of the coatings decreased, which was inversely proportional to the adhesion of the coatings.

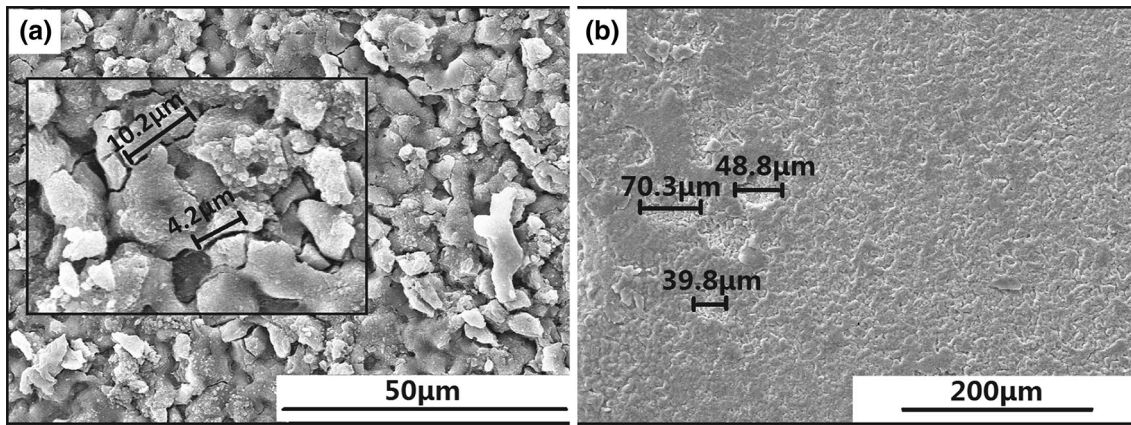


Fig. 5 Surface morphologies of the coating at 4.0 g/L after the thermal shock tests: (a) 3000 times, (b) 500 times

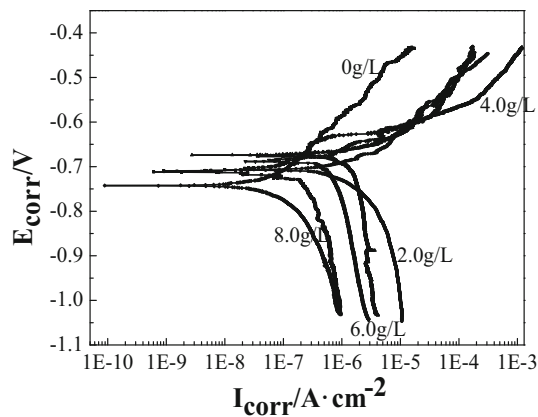


Fig. 6 Polarization curves of MAO coatings at different Al_2O_3 micro-powder concentrations

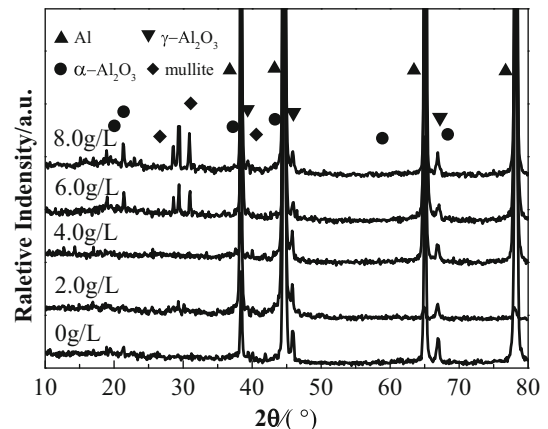


Fig. 7 XRD spectra of MAO coatings at different Al_2O_3 micro-powder concentrations

In addition, the coatings were thicker than the coating without Al_2O_3 micro-powder. It was also beneficial for the adhesive strength between the substrates and coatings. Therefore, the coatings with the addition of Al_2O_3 micro-powder exhibited relatively excellent adhesion during the scratch tests.

There was no visible crack or peeling on the coating surface of the specimens with the temperature at 500 °C for 50 cycles except at 4.0 g/L. Figure 5(a) and (b) exhibits the surface morphologies of the MAO coating at 4.0 g/L under different magnification times (3000 times and 500 times) after the thermal shock tests. Cracks spread over the surface with the size from a few microns to 10 μm (Fig. 5a) and some peelings with the diameter about tens of microns off of the coating occurred (Fig. 5b). The thermal shock parameter $R = k \sigma (1 - \nu) / \alpha E$, where k is thermal conductivity, σ is fracture stress, ν is Poisson's ratio, α is linear coefficient thermal expansion, E is Young's modulus, reveals the influential factors of thermal shock resistance of materials (Ref 14). The SEM results in Fig. 2 indicated that the thickest coating at 4.0 g/L was less porous in comparison with 0 g/L, 2.0 g/L and relatively denser than 6.0 g/L, 8.0 g/L. The special microstructure at 4.0 g/L was thought to be associated with the low thermal conductivity and high Young's modulus. Meanwhile, the special microstructure was bad for the absorption of thermal shock energy and restrained the release of thermal stress of the interface area, which was caused by the different coefficients of the thermal

expansion (Ref 15) between Al_2O_3 and Al substrate at 500 °C (around $8.7 \times 10^{-6}/^\circ\text{C}$ and $23.8 \times 10^{-6}/^\circ\text{C}$, respectively). Hence, the thermal shock parameter R decreased at 4.0 g/L and the initiation of the micro-cracks between the coatings and substrate under the cyclic heating condition occurred. Furthermore, the cross-sectional morphologies in Fig. 2 had showed some original strip cracks distributed in the coatings only at 4.0 g/L (Fig. 2f). When the initial micro-cracks of the interface area and the original strip cracks in the coatings connected, the propagation of the cracks induced the peelings off of the coating under the severe thermal shocking.

Polarization curves of different specimens in 3.5% NaCl solution are shown in Fig. 6, which indicates that the corrosion potential increased at first and then decreased, and the corrosion current density kept increasing slowly. The corrosion resistance was determined by the coating thickness and coating morphologies. Corrosion potential grew with the increase in the coating thickness; the corrosion current density went up because some strip cracks existed in the MAO coatings. The fitting corrosion rates of the MAO coatings increased gradually and the results were 6.6×10^{-3} , 1.61×10^{-2} , 1.78×10^{-2} , 2.19×10^{-2} , 4.81×10^{-2} mm/a, respectively. All the factors above showed that the corrosion resistance decreased ultimately.

The phases of MAO coatings at different Al_2O_3 micro-powder concentrations are indicated in Fig. 7. It was observed that the addition of Al_2O_3 micro-powder had less effect on the

main phases which were proved to be γ - Al_2O_3 , mullite and little α - Al_2O_3 . There were some intense aluminum signals which came from the substrate of aluminum alloy. The more Al_2O_3 micro-powder additives added, the more α - Al_2O_3 and mullite generated. The mullite ($3\text{Al}_2\text{O}_3 \cdot 2\text{SiO}_2$) was fabricated by the reactions between the electrolyte and the Al_2O_3 under the effect of the high temperature and pressure, which demonstrated that the Al_2O_3 micro-powder additives efficiently involved in the MAO coating formation, in agreement with the results of surface morphologies and EDS.

4. Conclusions

Al_2O_3 micro-powder with negative surface charge entered in the coating holes under the interaction of electric field and mechanical stirring. The absorbed Al_2O_3 micro-powder was melted by the micro-arcs and formed the MAO coatings in collaboration with the Al_2O_3 produced by substrate oxidation. With the increase of Al_2O_3 micro-powder, the oxidation voltages, micro-hardness and the thickness of the coatings went up firstly and decreased ultimately which raised the coating formation efficiency. Although the adhesion between the substrate and the MAO coatings improved with the addition of Al_2O_3 micro-powder, the coatings still peeled easily from the specimen at 4.0 g/L, because the existence of the original micro-cracks absorbed more thermal shock energy and then resulted in the coalescence and propagation of the cracks which triggered the peelings off of the coating. When the concentration of Al_2O_3 micro-powder increased, the micropore sizes on coating surface decreased, the coating surface became smooth and the corrosion rates increased gradually. MAO coatings mainly consisted of γ - Al_2O_3 , mullite and little α - Al_2O_3 .

Acknowledgments

The present work was supported by the Scientific Research Starting Project (2015QHZ020) and Open Fund (X151515KCL16) of Sichuan Province University Key Laboratory of oil and gas field material, Southwest Petroleum University.

References

1. V. Shoaie-Rad, M.R. Bayati, H.R. Zargar, J. Javadpour, and F. Golestani-Fard, In situ growth of ZrO_2 - Al_2O_3 nano-crystalline ceramic coatings via micro arc oxidation of aluminum substrates, *Mater. Res. Bull.*, 2012, **47**(6), p 1494–1499
2. A. Venugopal, R. Panda, S. Manwatkar, K. Sreekumar, L. Rama Krishna, and G. Sundararajan, Effect of micro arc oxidation treatment on localized corrosion behaviour of AA7075 aluminum alloy in 3.5% NaCl solution, *Trans. Nonferrous Met. Soc. China*, 2012, **22**(3), p 700–710
3. J. Li, H. Cai, X. Xue, and B. Jiang, The outward-inward growth behavior of microarc oxidation coatings in phosphate and silicate solution, *Mater. Lett.*, 2010, **64**(19), p 2102–2104
4. L. Wen, Y. Wang, Y. Zhou, L. Guo, and J.H. Ouyang, Microstructure and corrosion resistance of modified 2024 Al alloy using surface mechanical attrition treatment combined with microarc oxidation process, *Corros. Sci.*, 2011, **53**(1), p 473–480
5. D.E. Lozano, R.D. Mercado-Solis, A.J. Perez, J. Talamantes, F. Morales, and M.A.L. Hernandez-Rodriguez, Tribological behaviour of cast hypereutectic Al-Si-Cu alloy subjected to sliding wear, *Wear*, 2013, **301**(s1–4), p 434–443
6. G. Sabatini, L. Ceschini, C. Martini, J.A. Williams, and I.M. Hutchings, Improving sliding and abrasive wear behaviour of cast A356 and wrought AA7075 aluminium alloys by plasma electrolytic oxidation, *Mater. Des.*, 2010, **31**(2), p 816–828
7. D. Shen, G. Li, C. Guo, J. Zou, J. Cai, and D. He, Microstructure and corrosion behavior of micro-arc oxidation coating on 6061 aluminum alloy pre-treated by high-temperature oxidation, *Appl. Surf. Sci.*, 2013, **287**, p 451–456
8. L. Gorjan, G. Blugan, M. Boretius, S. De La Pierre, M. Ferraris, and V. Casalegno, Fracture behavior of soldered Al_2O_3 ceramic to A356 aluminum alloy and resistance of the joint to low temperatures exposure, *Mater. Des.*, 2015, **88**, p 889–896
9. Y.L. Song, X.Y. Sun, and Y.H. Liu, Effect of TiO_2 nanoparticles on the microstructure and corrosion behavior of MAO coatings on magnesium alloy, *Mater. Corros.*, 2012, **63**(9), p 813–818
10. X. Li and B.L. Luan, Discovery of Al_2O_3 particles incorporation mechanism in plasma electrolytic oxidation of AM60B magnesium alloy, *Mater. Lett.*, 2012, **86**, p 88–90
11. P. Wang, X.Y. Guo, and X.L. Mao, Influences of vanadium doping on structure and performance of aluminum alloy micro-arc oxidation coating, *Rare. Met. Mater. Eng.*, 2014, **43**(7), p 1759–1763 ([in Chinese])
12. D. Shen, G. Li, C. Guo, J. Zou, J. Cai, and D. He, Microstructure and corrosion behavior of micro-arc oxidation coating on 6061 aluminum alloy pre-treated by high-temperature oxidation, *Appl. Surf. Sci.*, 2013, **265**, p 431–437
13. H.X. Li and R.G. Song, Effects of nano-additive TiO_2 on performance of micro-arc oxidation coatings formed on 6063 aluminum alloy, *Trans. Nonferrous Met. Soc. China*, 2013, **23**, p 406–412
14. Y. Zhong, L. Shi, M. Li, F. He, and X. He, Characterization and thermal shock behavior of composite ceramic coating doped with ZrO_2 particles on TC4 by micro-arc oxidation, *Appl. Surf. Sci.*, 2014, **311**, p 158–163
15. Z. Jiang, X. Zeng, and Z. Yao, Preparation of micro-arc oxidation coatings on magnesium alloy and its thermal shock resistance property, *Rare Met.*, 2006, **25**(3), p 270–273